Beam Test Measurements with Planar and 3D Silicon Strip Detectors Irradiated to sLHC Fluences

Michael Köhler, Liv Wiik, Richard Bates, Gian-Franco Dalla Betta, *Senior Member, IEEE,* Celeste Fleta, Jaakko Härkönen, Karl Jakobs, Manuel Lozano, Teppo Mäenpää, Henri Moilanen, Chris Parkes, Ulrich Parzefall, Giulio Pellegrini, Leonard Spiegel

***Abstract*—The planned luminosity upgrade of the CERN LHC to the super LHC (sLHC) requires investigation of new radiation hard tracking detectors. Compared to the LHC, tracking detectors must withstand a 5-10 times higher radiation fluence. Promising radiation hard options are planar silicon detectors with n-side readout and silicon detectors in 3D technology, where columnar electrodes are etched into the silicon substrate. This article presents beam test measurements performed with planar and 3D n-in-p silicon strip detectors. The detectors were irradiated to different fluences, where the maximum fluence was 3×10^{15} 1 MeV neutron equivalent particles per square centimetre ($\mathrm{n_{eq}/cm^2}$) for the planar detectors and $2 \times 10^{15}\ \mathrm{n_{eq}/cm^2}$for the 3D detectors. In addition to signal measurements, charge sharing and resolution of both detector technologies are compared. An increased signal from the irradiated 3D detectors at high bias voltages compared to the signal from the unirradiated detector indicates that charge multiplication effects occur in the 3D detectors. At a bias voltage of 260 V, the 3D detector irradiated to $2 \times 10^{15}\ \mathrm{n_{eq}/cm^2}$ yields a signal almost twice as high as the signal of the unirradiated detector. Only 30 % of the signal of an unirradiated detector could be measured with the planar detector irradiated to $3 \times 10^{15}\ \mathrm{n_{eq}/cm^2}$ at a bias voltage of 600 V, which was the highest bias voltage applied to this sensor.**

I. Introduction

THE super LHC (sLHC) [1] will deliver a peak instantaneous luminosity of approximately $5 \times 10^{34}\,\mathrm{cm^{-2}s^{-1}}$. In the ATLAS detector [2], after collecting an integrated luminosity of $3000\,\mathrm{fb^{-1}}$, this will lead to a radiation fluence of around 10^{15} 1 MeV neutron equivalent particles per square centimetre ($\mathrm{n_{eq}/cm^2}$) in the inner layers foreseen to equip with strip detectors and even more than $10^{16}\,\mathrm{n_{eq}/cm^2}$ in the innermost pixel detector layer [3]. While ionising radiation leads to surface damage due to accumulation of oxide charge, Non Ionising Energy Loss (NIEL) induced by fast hadrons leads to bulk damage and constitutes the main cause of radiation damage in silicon detectors. Bulk damage increases the depletion voltage, trapping of free charge carriers and the leakage current. The increases are, to a good approximation, proportional to the radiation fluence [4], [5], although indications for deviations in highly irradiated silicon detectors have been observed [6]. At fluences of the order of $10^{15}\,\mathrm{n_{eq}/cm^2}$, the depletion voltage for planar $300\,\mu\mathrm{m}$ thick silicon detectors exceeds the voltage at which the detectors can be operated using the current LHC power services. This effect and especially the increase of the trapping probability lead to a severe signal degradation.

An option for radiation hard detectors are silicon sensors with n-side readout in p-type float-zone substrate [7]. The signal degradation is reduced compared to detectors where the readout junction electrodes are formed by segmented p-electrodes. The substrate of n-in-p float-zone detectors does not undergo type inversion after irradiation and hence the region with the high electric field remains at the structured side, where the maximum of the weighting field is located, before and after irradiation. Furthermore, electrons are accelerated towards the readout side, into the region of the high weighting field. Therefore, the measured signal is dominated by electrons, which have a lower trapping probability compared to holes [5].

To increase radiation hardness by a modified detector geometry, 3D detectors have been proposed [8]. In this design, columnar electrodes are etched into the silicon substrate perpendicularly to the surface. These columns are doped to form readout junction electrodes and ohmic electrodes. The distance for drift of generated charge carriers and for depletion is given by the spacing between columnar electrodes of opposite doping types rather than by the detector thickness as in planar detectors. Therefore, enhanced radiation hardness is expected due to reduced trapping and a reduced depletion voltage, while the total ionised charge is determined by the substrate thickness. In addition to the original concept with columns passing through the entire detector [8], a simplified technology of 3D detectors is under study, known as double-sided 3D detectors. In double-sided 3D detectors (or 3D-DDTC, Double-Sided Double Type Column) [9], [10] the columns are etched from the front and the back into the wafer and do not penetrate the wafer completely. This approach requires less processing steps, however, the performance is expected to be similar to full 3D detectors. Detectors in double-sided 3D technology with columns only partially etched into the silicon are manufactured by IMB-CNM [9], [11] and by FBK-irst [10], [12]. Full 3D

M. Köhler, L. Wiik, K. Jakobs and U. Parzefall are with the Institute of Physics, University of Freiburg, 79104 Freiburg, Germany (e-mail: michael.koehler@physik.uni-freiburg.de).

R. Bates and C. Parkes are with the Department of Physics and Astronomy, Glasgow University, Glasgow G12 8QQ, UK.

G.-F. Dalla Betta is with the Department of Information Engineering and Computer Science, University of Trento and INFN, Sezione di Padova (Gruppo collegato di Trento), I-38123 Povo di Trento (TN), Italy.

C. Fleta, M. Lozano and G. Pellegrini are with the Centro Nacional de Microelectronica (IMB-CNM, CSIC), 08193 Bellaterra, Barcelona, Spain.

J. Härkönen, T. Mäenpää and H. Moilanen are with the Helsinki Institute of Physics (HIP), FIN-00014 Helsinki, Finland.

L. Spiegel is with the Fermi National Accelerator Laboratory, PO Box 500, MS 121, Batavia, IL 60510, USA.

Operated by Fermi Research Alliance, LLC under Contract No. De-AC02-07CH11359 with the United States Department of Energy.

detectors with columns penetrating through the entire substrate are produced by the Stanford Nanofabrication Facility [13] and SINTEF [14].

This article describes comparative beam test measurements of n-in-p silicon strip detectors produced in planar technology and in double-sided 3D technology. To investigate the behaviour after irradiation, the detectors have been irradiated to the radiation fluences expected for the sLHC strip detector layers. While beam test measurements with unirradiated double-sided 3D strip detectors [15] proved the maturity of the design, the measurements reported here focus on properties after irradiation. Those include signal measurements, studies on charge sharing and resolution measurements. While these measurements were performed with high-energy particles, results from measurements with identical irradiated 3D silicon strip detectors using a radioactive source and an infrared laser setup are reported in [16]. A description of charge collection measurements using various planar silicon sensors performed with a radioactive source can be found in [17].

II. Devices Under Test

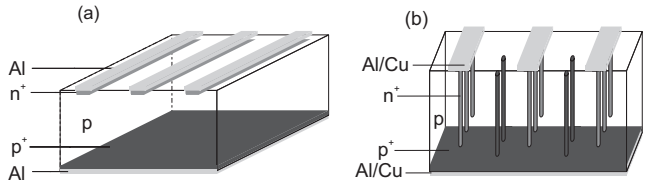

Fig. 1: Principle design of (a) planar strip detectors and (b) double-sided 3D strip detectors (not to scale). P-stop implantations, which are present between the strips in the planar design and around each n^+-doped column in the 3D design, are omitted.

A. Planar Detectors

Planar silicon strip sensors (see Fig. 1(a)), named ATLAS07, were designed by the ATLAS Silicon Strip Sensor Upgrade collaboration and fabricated by Hamamatsu Photonics [18]. The sensors were manufactured on p-type float-zone material with n^+-doped readout strips. The substrate material has a resistivity of $\sim 6.7\ \mathrm{k\Omega\cdot cm}$. The $1\,\mathrm{cm} \times 1\,\mathrm{cm}$ miniature strip sensors used in this beam test have a thickness of $320\,\mu\mathrm{m}$ and a strip pitch of $74.5\,\mu\mathrm{m}$. Each miniature sensor comprises 104 strips with a length of $8\,\mathrm{mm}$. In contrast to the 3D detectors described in the following section, the planar sensors were made with an integrated AC-coupling structure. For the sensors used the strip metallisation is wider than the n-strip implant. Both p-spray and p-stop isolation schemes were used on the sensors in the beam test. Further details on the design, including strip isolation structures, are given in [19].

B. 3D Detectors

The 3D detectors under test were designed by the University of Glasgow and IMB-CNM (Barcelona, Spain) [11] and produced by IMB-CNM in a double-sided processing technology on p-type substrate [9], see Fig. 1(b). The substrate consists of float-zone silicon with a resistivity of 1 to $5\ \mathrm{k\Omega\cdot cm}$. Junction columns ($\mathrm{n}^+$-doped) are etched into the wafer from the front side and p^+-doped ohmic columns are etched from the back. The ohmic columns are periodically arranged in the middle of four junction columns. On the surface, all junction columns in a row are connected by means of a metallisation layer. On the back, a p^+-doped polysilicon layer with a metallisation layer connects all ohmic columns. Neither set of columns in the double-sided 3D detectors penetrates the wafer entirely. All columns have a depth of $250\,\mu\mathrm{m}$, whereas the substrate is $285\,\mu\mathrm{m}$ thick. The columns are partially filled with polysilicon and passivated with a TEOS layer. The columns have a diameter of approximately $10\,\mu\mathrm{m}$.

Each 3D detector consists of 50 strips with a pitch of $80\,\mu\mathrm{m}$, each of the strips has a length of $4\,\mathrm{mm}$. Each of this strips is connected to an individual channel of the readout chip via a pitch-adapter with integrated bias resistors and decoupling capacitors to achieve AC-coupling. The active area is surrounded by a 3D guard ring consisting of n^+ and p^+ columns. To provide isolation of the strips after radiation-induced accumulation of oxide charges, each n^+ column is surrounded by a p-stop implantation on the front side. Additionally, a p-stop implantation surrounds the active area of the entire detector.

C. Irradiations

The devices under test were irradiated with $25\,\mathrm{MeV}$ protons at the Karlsruhe Compact Cyclotron. During the irradiation the devices were kept unbiased. The fluences received by the detectors are listed in Table I. The values are scaled to $1\,\mathrm{MeV}$ equivalent neutrons ($\mathrm{n_{eq}/cm^2}$) using the NIEL hypothesis with a hardness factor of 1.85. For each fluence, a relative error of 20% is assumed. The planar detector irradiated with a fluence $5\times10^{13}\,\mathrm{n_{eq}/cm^2}$ is regarded as lightly irradiated since no significant radiation damage leading to a lower signal is expected for this comparatively low fluence. No annealing has been performed on purpose, however the devices under test were stored at room temperature between preparation and the measurements for a maximum of three days.

TABLE I: Irradiation fluences of the devices under test.

	Planar	3D
Fluence ($\mathrm{n_{eq}/cm^2}$)	5×10^{13}	0
	1×10^{15}	1×10^{15}
	3×10^{15}	2×10^{15}

III. Beam Test Setup

The beam test was performed at the CERN SPS H2 beamline in July 2009 using $225\ \mathrm{GeV}$ pions. These can be regarded as minimum ionising particles and deposit the same amount of energy as high-energy particles which are typically considered for reconstruction in high-energy physics experiments. Reference tracks for the devices under test were given by the Silicon Beam Telescope (SiBT) [20], [21], which has a nominal resolution of $4\ \mu\mathrm{m}$. The SiBT consists of 8

reference planes made by planar silicon microstrip sensors. Due to the sensors being oriented at an angle of 90° to each other, the SiBT delivers 4 space points. The SiBT is placed inside a thermally insulated and temperature controlled box, which can be cooled down to temperatures as low as $-25^\circ\mathrm{C}$ using Peltier elements. This temperature corresponds approximately to the sensor target temperature of $-20^\circ\mathrm{C}$, which is foreseen for the strip detector layers of the sLHC ATLAS upgrade. The sensors were placed perpendicular to the beam, and triggered by two scintillators placed on either side of the setup. The readout electronics and the data acquisition is based on CMS Tracker prototype components. Hence the telescope detectors and the devices under test are read out by APV25 chips [22] operated in peak mode with a $50\,\mathrm{ns}$ shaping applied, synchronised to a $40\ \mathrm{MHz}$ clock.

IV. Calibration and Data Preparation

The detector signals, measured in ADC counts, are converted into charge exploiting the well known signal spectrum of the planar telescope sensors. The most probable value of a Landau distribution, obtained from a fit of a Landau function convoluted with a Gaussian, is calculated for the signal spectrum of the telescope detectors. To obtain the calibration factor, this value is equated with the expected charge deposited by high-energy particles in silicon of the given thickness. The relative error of the calibration is estimated as 8%, consisting of the thickness tolerance of the reference detectors, variations of the signal measured with different reference detectors and variations between different measurement runs. The expected signal of the planar detectors under test, which have a thickness of $(320 \pm 20)\,\mu\mathrm{m}$, is $(24.7 \pm 1.6)\,\mathrm{ke}^-$, whereas the 3D detectors with a thickness of $(285 \pm 15)\,\mu\mathrm{m}$ are expected to yield a signal of $(21.9 \pm 1.2)\,\mathrm{ke}^-$.

The raw data of the detectors under study suffered from high common mode noise, which varies strongly and which causes substantial broadening of the signal spectra. To reduce these effects, a second order common mode subtraction was performed per event. However, the common mode contributions could not be fully removed, especially in the data of the irradiated 3D detectors.

V. Results

A. Measured Signal

A clustering algorithm was used to determine the signal of the detectors in the beam test. First, the channel with the highest signal-to-noise ratio is calculated and hits are accepted if the signal-to-noise ratio exceeds 5. To suppress noise clusters, the search for the seed strip is limited to the strip where the track is pointing to and two neighbours on either side. The signals of neighbouring channels are added as long as their signal-to-noise ratio is larger than 3. In the following investigation, track impact positions across the entire sensor surfaces are considered. However, tracks impinging close to dead or noisy strips are excluded.

A comparison of the signal spectra measured at a bias voltage of $500\,\mathrm{V}$ for the planar sensor irradiated to a fluence of $5 \times 10^{13}\,\mathrm{n_{eq}/cm^2}$ and the planar sensor irradiated to $3 \times 10^{15}\,\mathrm{n_{eq}/cm^2}$ is shown in Fig. 2(a). Both spectra are fitted with a convolution of a Landau function and a Gaussian, which describe the spectra well. The lightly irradiated sensor has, as expected, a higher most probable value compared to the sensor irradiated to $3 \times 10^{15}\,\mathrm{n_{eq}/cm^2}$. The bias voltage of $500\,\mathrm{V}$ was chosen as a reference point for the planar sensors as it equals the current limit of the existing ATLAS SCT voltage supply.

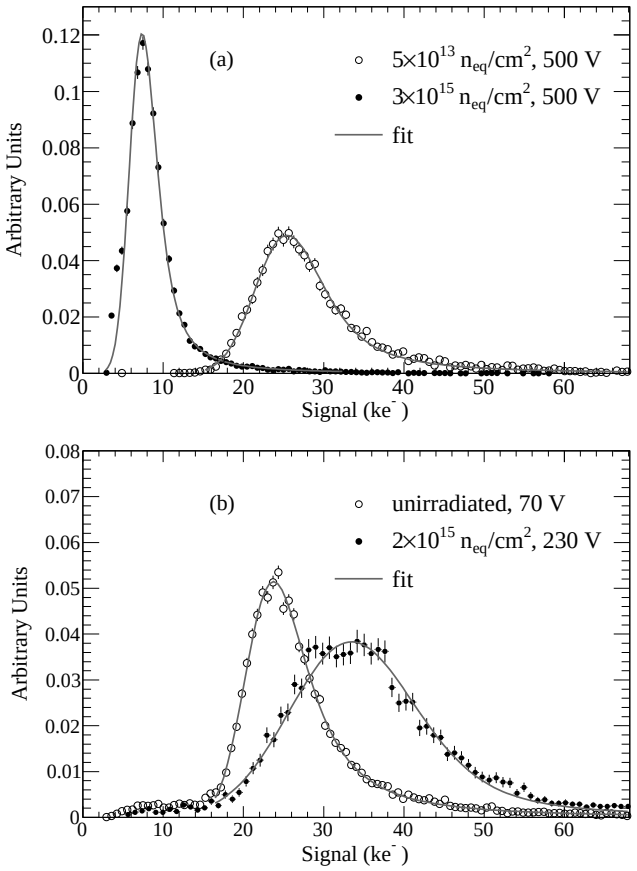

Fig. 2: Normalised signal distributions for different irradiation fluences, (a) measured with planar detectors and (b) measured with 3D detectors. The fit superimposed is a convolution of a Landau function and a Gaussian.

The signal of the planar sensors as a function of the bias voltage is summarised in Fig. 3(a). Due to the limited cooling power available in the beam test setup the voltages were selected in order to comply with a safe current limit of the detectors. The sensor irradiated to $5 \times 10^{13}\,\mathrm{n_{eq}/cm^2}$ yields a maximum signal of $(24.2 \pm 1.8)\,\mathrm{ke}^-$ at a bias voltage of $500\,\mathrm{V}$, corresponding to the expected charge liberated by a minimum ionising particle passing through $320\,\mu\mathrm{m}$ of silicon. The plateau of the signal is already measured at $200\,\mathrm{V}$, which is above the full depletion voltage of the sensor.

Both planar sensors irradiated to higher fluences show a clear degradation in charge collection efficiency. The signal of the sensor irradiated to $1 \times 10^{15}\,\mathrm{n_{eq}/cm^2}$ rises from $(11.6 \pm 0.9)\,\mathrm{ke}^-$ at $500\,\mathrm{V}$ to $(17.7 \pm 1.4)\,\mathrm{ke}^-$ at $950\,\mathrm{V}$, which is the highest voltage applied to this sensors during the beam test. The sensor irradiated to $3 \times 10^{15}\,\mathrm{n_{eq}/cm^2}$ collects $(6.8 \pm 0.5)\,\mathrm{ke}^-$ at a bias voltage of $500\,\mathrm{V}$.

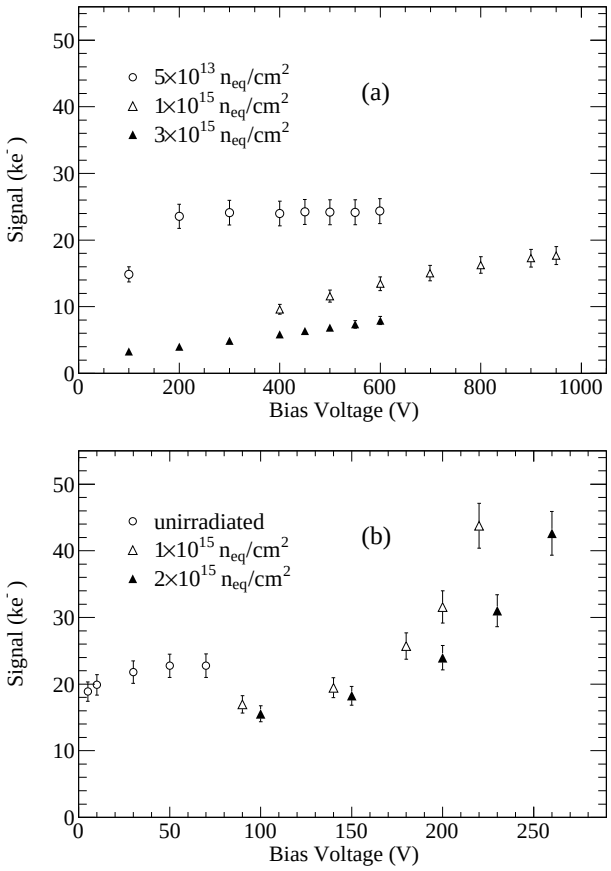

Fig. 3: Signal as a function of the applied bias voltage for different irradiation fluences, (a) measured with the planar sensors and (b) measured with the 3D sensors. The errors are dominated by a systematic contribution due to the calibration uncertainty.

The full depletion voltage V_{dep} of the planar sensors can be approximated by [4]

$$V_{\mathrm{dep}} \approx \frac{q_0 d^2}{2\epsilon_0 \epsilon_r} g_C \, \Phi_{\mathrm{eq}}, \tag{1}$$

where q_0 is the elementary charge, d is the detector thickness and ϵ_0 and ϵ_r are the permittivity of vacuum and silicon, respectively. A linear dependence on the irradiation fluence Φ_{eq} is assumed. With the acceptor introduction rate $g_C = 0.012\,\mathrm{cm}^{-1}$ [23] for protons in p-type float-zone silicon, $V_{\mathrm{dep}} \approx 900\,\mathrm{V}$ at $\Phi_{\mathrm{eq}} = 1 \times 10^{15}\,\mathrm{n_{eq}/cm^2}$ and $V_{\mathrm{dep}} \approx 2800\,\mathrm{V}$ at $\Phi_{\mathrm{eq}} = 3 \times 10^{15}\,\mathrm{n_{eq}/cm^2}$ are expected. Although eq. 1 is only valid after beneficial annealing, which was not performed for the sensors investigated here, it serves as an estimate. Therefore, the highest bias voltage applied to the sensor irradiated to $1 \times 10^{15}\,\mathrm{n_{eq}/cm^2}$ is in the order of the estimated full depletion voltage, whereas the full depletion voltage could not be reached for the sensor irradiated to $3 \times 10^{15}\,\mathrm{n_{eq}/cm^2}$.

The signal measured with the irradiated 3D detectors at high bias voltages substantially exceeds the signal of the unirradiated detector, see Fig. 3(b). At $70\,\mathrm{V}$, the highest voltage applied, the unirradiated 3D detector yields a signal of $(22.8 \pm 1.8)\,\mathrm{ke^-}$, which is in agreement with the charge liberated by a high-energy particle passing through silicon of the given thickness. The signal reaches a plateau already at $50\,\mathrm{V}$. This is in agreement with the full depletion voltage, which is approximately $40\,\mathrm{V}$ [16]. The signals measured with the irradiated 3D detectors exceed the signal of the unirradiated detector and increase strongly for voltages above approximately $150\,\mathrm{V}$. At the highest bias voltages applied, $220\,\mathrm{V}$ for the sensor irradiated to $1 \times 10^{15}\,\mathrm{n_{eq}/cm^2}$ and $260\,\mathrm{V}$ for the sensor irradiated to $2 \times 10^{15}\,\mathrm{n_{eq}/cm^2}$, the signal is approximately twice as high as the signal of the unirradiated sensor. The fact that more charge is measured than liberated by the penetrating particle can be attributed to charge multiplication due to impact ionisation. Indications for charge multiplication in irradiated 3D silicon strip detectors were also observed in measurements using a radioactive source and an infrared laser setup [16], [24]. When free charge carriers are accelerated by a sufficiently high electric field in between collisions, they can gain enough energy to create additional electron-hole pairs. For substantial charge multiplication electric fields higher than $10\,\mathrm{V/\mu m}$ are required [25]. The multiplication of holes requires higher electric fields than the multiplication of electrons. These measurements provide evidence that the radiation-induced increase of the effective doping concentration leads to electric field strengths sufficiently high for strong charge multiplication. This effect has also been observed with highly irradiated planar silicon strip detectors [26], [6] and epitaxial silicon pad detectors [27], where higher voltages due to a larger spacing between the electrodes are needed. The specific geometry and the short distance of about $50\,\mu\mathrm{m}$ between junction columns and ohmic columns in the 3D detectors investigated here leads to a high electric field and therefore to strong charge multiplication already at comparatively low voltages. Charge multiplication has not been observed in unirradiated silicon detectors designed for high-energy particle physics applications. Since the operating voltage was limited in this beam test, onset of charge multiplication effects in the planar strip detectors could not be conclusively observed.

A comparison of the signal spectra of the 3D detectors in Fig. 2(b) shows that the spectrum of the detector irradiated to $2 \times 10^{15}\,\mathrm{n_{eq}/cm^2}$, where charge multiplication occurs, has a higher most probable value and a larger width than the spectrum of the unirradiated detector. In addition to higher noise, the broadening of the spectrum is caused by a common mode contribution which could not be completely subtracted and effectively increases the measured noise. A further broadening is caused by the dependence of the signal on the track impact point, as will be discussed in Section V-B. The spectra shown in Fig. 2 are generated by tracks having impact points all across the sensor. The lower tail of the distribution, below approximately $15\,\mathrm{ke^-}$, is caused by tracks going directly through the passive columns and therefore leading to lower signal [15].

The measured signal and the leakage current of the irradiated 3D detectors are strongly correlated, as shown in Fig. 4. The measurement of the leakage current was performed at approximately $-20^{\circ}\mathrm{C}$ and reflects the current drawn by all strips, as the current flowing through the guard ring has been

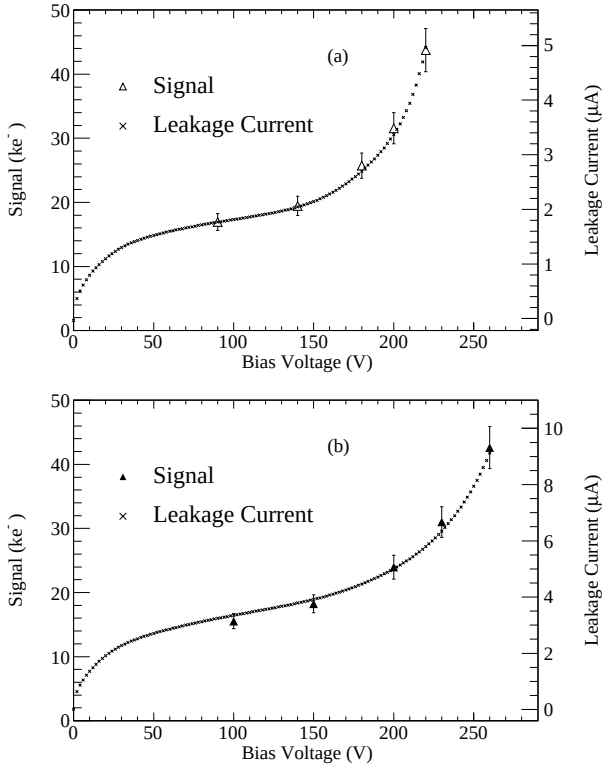

Fig. 4: Overlay of the measured signal and the leakage current, (a) for the 3D detector irradiated to $1 \times 10^{15}\,\mathrm{n_{eq}/cm^2}$ and (b) for the 3D detector irradiated to $2\times10^{15}\,\mathrm{n_{eq}/cm^2}$. The leakage current was measured at $-20\,^{\circ}\mathrm{C}$.

subtracted. The guard ring current accounted for 10%-15% of the total current. After tending to saturate at about $50\,\mathrm{V}$, the leakage current increases strongly above $150\,\mathrm{V}$, in agreement with the signal curves. Charge carriers generated both by traversing particles and by thermal excitation are multiplied by the same factor as soon as the electric field is sufficiently high.

B. Space-Resolved Signal

The drift path for liberated charge carriers towards the electrodes in 3D detectors depends strongly on the impact position of the particle track. Both the drift length and the electric field along the drift path are affected by the position where the charge carriers are created. Given the periodic structure of the detector and considering a square unit cell with the junction column in the centre and the ohmic columns in the corners, regions with particularly low and high electric field can be identified, see Fig. 5. Regions with the lowest electric field are located in the middle between the columnar electrodes of the same doping type, see Fig. 5(a). Distinct high field regions are located on the direct connection between a junction column and an ohmic column, see Fig. 5(b). Tracks impinging on the low field regions located at the left and right margins of the unit cell lead to higher charge sharing between neighbouring readout strips. As the effects of charge sharing should be separated from the following discussion, these tracks are not considered.

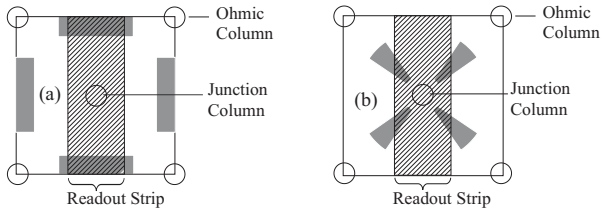

Fig. 5: Sketch of the unit cell of a 3D detector with the readout strip, represented as the hatched region, running vertically. In (a) regions with low electric field and in (b) regions with high electric field are shown as grey shaded areas (see text).

While the signal for tracks impinging in the two distinct regions does not differ in the unirradiated 3D detector, substantial differences are measured for the irradiated sensors. The signal of tracks impinging on the high field region and the low field region are shown as a function of the applied bias voltage in Fig. 6 for the 3D detectors irradiated to $1 \times 10^{15}\,\mathrm{n_{eq}/cm^2}$ and $2\times10^{15}\,\mathrm{n_{eq}/cm^2}$. Results from the measurements at lower voltages are not included as the limited number of tracks does not allow a statistically significant investigation. A difference of the signal measured for tracks impinging in the distinct regions can be clearly identified. Charge carriers generated in both regions evidently undergo charge multiplication. The results indicate that the multiplication takes place only in a thin region around the junction column. Otherwise a higher multiplication for charge carriers generated in the low field region, which have a longer drift path, would be expected. Several effects lead to the observed signal non-uniformity. In the low field region the charge carriers have longer drift distances and lower drift velocities resulting in a higher trapping probability. Furthermore, as the charge multiplication coefficients exhibit a strong dependence on the electric field [25], the charge carriers drifting along a path with a higher electric field have a larger probability of being multiplied. The difference between the signals in the distinct regions increases with increasing voltage.

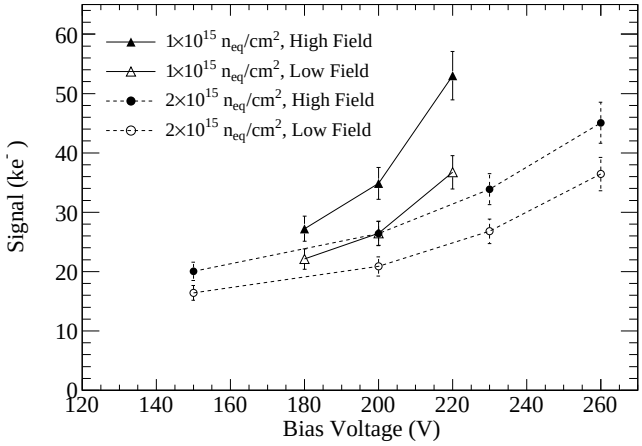

Fig. 6: Signals in the regions with low and high electric field as a function of the applied bias voltage for the 3D detectors irradiated to $1 \times 10^{15}\,\mathrm{n_{eq}/cm^2}$ and $2 \times 10^{15}\,\mathrm{n_{eq}/cm^2}$. The lines connecting the data points are shown to guide the eye.

C. Charge Sharing

The different electric field configurations in planar and 3D detectors affect the magnitude of charge sharing between neighbouring readout strips. In planar detectors the liberated charge carriers drift parallel to the border between readout strips. Transverse diffusion during the drift leads to broadening of the charge cloud in the plane of the readout strips and increases the probability of charge sharing. In contrast to that, the electric field in 3D detectors is dominated by a component perpendicularly to the border between readout strips. Therefore, the charge sharing probability is not increased by transverse diffusion and it is less pronounced than in planar detectors. A comparison of charge sharing in 3D and planar detectors using synchrotron measurements is reported in [28]. While charge sharing can be exploited to increase the spatial resolution, it can also be disadvantageous when the signal-to-noise ratio is low and the broadening of the charge cloud leads to further decrease of the signal measured per readout channel. This is especially true for binary readout systems as envisaged for the upgrade of the ATLAS semiconductor tracker (SCT). Charge sharing reduces the detection efficiency if the total signal is not much higher than the threshold value.

The fraction of clusters consisting of more than one strip as a function of the distance to the readout strip centre is shown in Fig. 7(a) for the lightly irradiated planar detector (irradiation fluence $5 \times 10^{13}\,\mathrm{n_{eq}/cm^2}$) and in Fig. 7(b) for the unirradiated 3D detector. To calculate the cluster width, the clustering algorithm explained in Section V-A was applied. The data originate from measurements with bias voltages well above full depletion, $500\,\mathrm{V}$ for the planar detector and $70\,\mathrm{V}$ for the 3D detector. In both detectors, only tracks impinging close to mid-pitch exhibit a significant charge sharing probability. The width of the region with high charge sharing is visibly reduced in the 3D detector, where it is limited to a narrow band smaller than $10\,\mu\mathrm{m}$ at the left and right margin. In the planar detector this region extends up to $20\,\mu\mathrm{m}$. In total, 11% of the hits in the 3D detector and 35% of the hits in the planar detector are shared between neighbouring readout strips.

Due to comparable noise and signal values in the two detectors investigated, the signal-to-noise cuts applied for the clustering have essentially the same effects for both detectors. As the signal magnitudes alter strongly after irradiation and the cuts would be no longer comparable, the investigation of charge sharing is not extended to the detectors irradiated to higher fluences.

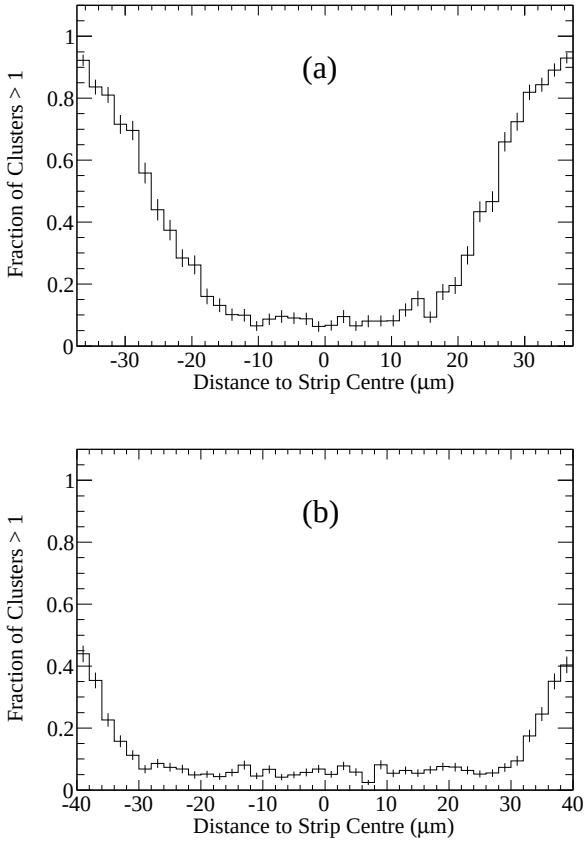

Fig. 7: Fraction of clusters consisting of more than one readout strip as a function of distance to the readout strip centre, (a) for the planar detector irradiated to $5 \times 10^{13}\,\mathrm{n_{eq}/cm^2}$ measured at $500\,\mathrm{V}$ and (b) for the unirradiated 3D detector measured at $70\,\mathrm{V}$.

D. Spatial Resolution

To assess tracking capabilities after irradiation, the spatial resolution is investigated. The standard deviation of the differences between the track location determined by the devices under test and the beam telescope quantifies the spatial resolution. The seed strip is determined as the strip having the highest signal-to-noise ratio among the strips where the track is pointing to and its direct neighbours on either side of the track position. Accordingly, the highest neighbour of the seed strip is determined. If the signal-to-noise ratio of this strip exceeds 3, the track position measured by the device under test is given by the charge weighted mean between the seed and its highest neighbour. Otherwise, the location is given by the centre of the seed strip. No eta correction is applied. Exploiting this interpolation gives the opportunity to improve the spatial resolution compared to the binary resolution of $\sigma_{bin} = \mathrm{Pitch}/\sqrt{12}$. Events are excluded if the strip where the track is pointing to or one of its direct neighbours is dead or has extraordinarily high noise.

The resolution as a function of applied bias voltage is shown in Fig. 8(a) for the planar detectors and in Fig. 8(b) for the 3D detectors. The track extrapolation uncertainty, which is approximately $4\,\mu\mathrm{m}$ and dominated by the telescope resolution, was not subtracted. Statistical errors are indicated. Due to the limited statistics remaining for the 3D sensor irradiated to $1 \times 10^{15}\,\mathrm{n_{eq}/cm^2}$, after excluding noisy or dead channels and their neighbours, the interpolation of the track position could not be exploited. Hence this detector was excluded from the analysis of the spatial resolution.

A beneficial effect on the resolution due to charge sharing is apparent for all three planar sensors. With a pitch of $74.5\,\mu\mathrm{m}$ a binary resolution of $21.5\,\mu\mathrm{m}$ is expected. The resolution as a function of the applied bias voltage for the lightly irradiated sensor (irradiation fluence $5 \times 10^{13}\,\mathrm{n_{eq}/cm^2}$) is

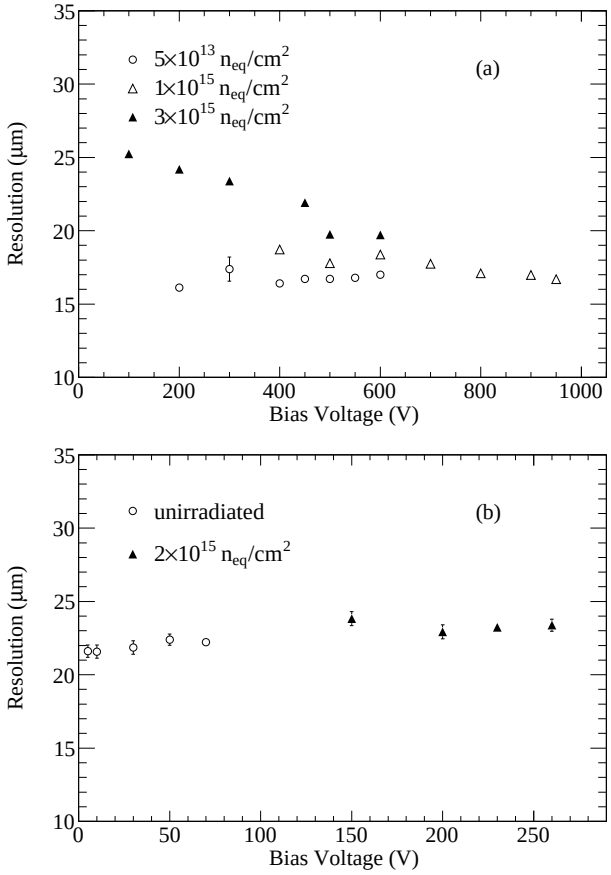

Fig. 8: Resolution versus applied bias voltage of (a) planar detectors and (b) 3D detectors irradiated to different fluences.

relatively constant and has a value of $(16.7 \pm 0.2)\,\mu\mathrm{m}$ at $500\,\mathrm{V}$. For the planar sensor irradiated to $1 \times 10^{15}\,\mathrm{n_{eq}/cm^2}$ the resolution improves with respect to the voltage leading to a resolution of $(16.7 \pm 0.2)\,\mu\mathrm{m}$ at $950\,\mathrm{V}$. This resolution is corresponding to the value measured for the sensor irradiated to $5 \times 10^{13}\,\mathrm{n_{eq}/cm^2}$. A large effect on the resolution due to irradiation is seen for the sensor which received the highest fluence, $3 \times 10^{15}\,\mathrm{n_{eq}/cm^2}$. At a bias voltage of $100\,\mathrm{V}$ the resolution is only $(25.2 \pm 0.2)\,\mu\mathrm{m}$. However increasing the bias voltage to $600\,\mathrm{V}$ leads to an improved resolution of $(19.7 \pm 0.1)\,\mu\mathrm{m}$. As mentioned in Section V-A this detector is not depleted at these voltages, so a further enhancement of the resolution could be expected at a higher bias voltage. The increase of the bias voltage increases the sensitive detector volume and leads to higher drift velocities of the charge carriers, which reduces the trapping probability. Both effects lead to a higher signal-to-noise ratio and to an improved resolution.

The resolution measured with the unirradiated 3D detector at $70\,\mathrm{V}$ is $(22.2 \pm 0.2)\,\mu\mathrm{m}$. Therefore, the binary resolution $23.1\,\mu\mathrm{m}$ can be slightly improved using the information of charge sharing, however to a lesser extent compared to the planar detectors due to reduced charge sharing in 3D detectors. This is expected from the charge sharing studies shown in Fig. 7. The detector irradiated to $2 \times 10^{15}\,\mathrm{n_{eq}/cm^2}$ yields a resolution of $(23.4 \pm 0.4)\,\mu\mathrm{m}$ at a bias voltage of $260\,\mathrm{V}$, which is somewhat worse than for the unirradiated sensor but still in agreement with the binary resolution. The resolution degrades slightly after irradiation. The increasing influence of charge multiplication for voltages higher than approximately $150\,\mathrm{V}$ does not negatively affect the resolution. Within the error margins, the resolution determined for the 3D detector irradiated to $2 \times 10^{15}\,\mathrm{n_{eq}/cm^2}$ does not depend on the bias voltage in the voltage range shown.

VI. Conclusion

The performance of irradiated planar and 3D silicon strip detectors was compared using beam test measurements. The signals of the irradiated 3D detectors exceed the signal measured with the unirradiated 3D detectors at high bias voltages significantly, which points to the occurrence of charge multiplication caused by impact ionisation. The signal of the unirradiated 3D detector is exceeded by the signal observed in the detectors irradiated to $1 \times 10^{15}\,\mathrm{n_{eq}/cm^2}$ and $2 \times 10^{15}\,\mathrm{n_{eq}/cm^2}$ already at $200\,\mathrm{V}$. However, the signal magnitude measured with the irradiated 3D detectors depends on the track impact position and is considerably less uniform than before irradiation. Considering that the bias voltage was limited during the beam test, the signal of the unirradiated planar detectors could not be reached with the irradiated planar detectors. Due to lower charge sharing in 3D detectors, a better spatial resolution could be obtained with the planar sensors. A degradation of the spatial resolution after irradiation was measured. The increasing influence of charge multiplication at high bias voltages does not lead to a significant degradation of the resolution of the 3D detector irradiated to $2 \times 10^{15}\,\mathrm{n_{eq}/cm^2}$.

Acknowledgement

This work was performed within the framework of the CERN RD50 Collaboration and the ATLAS Silicon Strip Sensor Upgrade Collaboration. The authors would like to thank Dr. A. Dierlamm and Prof. W. de Boer of the Karlsruhe Institute of Technology for performing the proton irradiations and the SPS crew for support during the beam test. This work is supported by the Initiative and Networking Fund of the Helmholtz Association, contract HA-101 ("Physics at the Terascale"). Also, this work has been partially supported by the Spanish Ministry of Education and Science through the GICSERV programme "Access to ICTS integrated nano- and microelectronics cleanroom".

References

[1] F. Gianotti *et al.*, "Physics potential and experimental challenges of the LHC luminosity upgrade," *Eur. Phys. J.,* vol. C39, pp. 293-333, 2005.

[2] G. Aad *et al.* [ATLAS Collaboration], "The ATLAS Experiment at the CERN Large Hadron Collider," *JINST,* vol. 3, S08003, 2008.

[3] I. Dawson, "Radiation predictions at the SLHC and irradiation facilities", presented at the *ATLAS Tracker Upgrade Workshop,* Liverpool, UK, Dec. 6-8, 2006 [Online]. Available: http://www.liv.ac.uk/physics/AHLUTW/

[4] G. Lindström *et al.*, "Radiation hard silicon detectors–developments by the RD48 (ROSE) collaboration", *Nucl. Instrum. Meth. A,* vol. 466, pp. 308-326, 2001.

[5] G. Kramberger, V. Cindro, I. Mandić, M. Mikuž, M. Zavrtanik, "Determination of effective trapping times for electrons and holes in irradiated silicon," *Nucl. Instrum. Meth. A,* vol. 476, pp. 645-651, 2002.

[6] G. Casse, A. Affolder, P.P. Allport, H. Brown, I. McLeod and M. Wormald, "Evidence of enhanced signal response at high bias voltages in planar silicon detectors irradiated up to $2.2 \times 10^{16}\,\mathrm{n_{eq}cm^{-2}}$," *Nucl. Instrum. Meth. A,* in press, doi: 10.1016/j.nima.2010.04.085.

[7] G. Casse, P.P. Allport, M. Hanlon, "Improving the radiation hardness properties of silicon detectors using oxygenated n-type and p-type silicon," *IEEE Trans. Nucl. Sci.,* vol. 47, no. 3, pp. 527-532, 2000.

[8] S. I. Parker, C. J. Kenney and J. Segal, "3D – A proposed new architecture for solid-state radiation detectors," *Nucl. Instrum. Meth. A,* vol. 395, pp. 328-343, 1997.

[9] G. Pellegrini, M. Lozano, M. Ullan, R. Bates, C. Fleta and D. Pennicard, "First double-sided 3-D detectors fabricated at CNM-IMB," *Nucl. Instrum. Meth. A,* vol. 592, pp. 38-43, 2008.

[10] A. Zoboli, G.-F. Dalla Betta, M. Boscardin, C. Piemonte, S. Ronchin, N. Zorzi and L. Bosisio, "Double-sided, double-type-column 3-D detectors: design, fabrication, and technology evaluation," *IEEE Trans. Nucl. Sci.,* vol. 55, no. 5, pp. 2775-2784, 2008.

[11] IMB-CNM, Instituto de Microelectrónica de Barcelona, Centro Nacional de Microelectrónica, 08193 Cerdanyola del Vallès (Bellaterra), Barcelona, Spain.

[12] FBK-irst, Fondazione Bruno Kessler, Povo - Via Sommarive 18, 38123 Trento, Italy.

[13] Stanford Nanofabrication Facility, 420 Via Palou Mall, Stanford, CA 94305 -407, USA.

[14] SINTEF, PO Box 124 Blindern, 0314 Oslo, Norway.

[15] M. Köhler *et al.*, "Beam test measurements with 3D-DDTC silicon strip detectors on n-type substrate," *IEEE Trans. Nucl. Sci.,* vol. 57, no. 5, pp. 2987-2994, 2010.

[16] R. Bates *et al.*, "Charge collection studies and electrical measurements of heavily irradiated 3D double-sided sensors and comparison to planar strip detectors," submitted to *IEEE Trans. Nucl. Sci.*, 2010.

[17] G. Casse, A. Affolder, P.P. Allport, M. Wormald, "Evaluation of floating zone and epitaxial planar silicon detectors with different substrate thickness after irradiation up to $2.2\times10^{16}\,\mathrm{n_{eq}cm^{-2}}$," *IEEE Trans. Nucl. Sci.,* vol. 56, no. 6, pp. 3752-3758, 2009.

[18] Hamamatsu Photonics K.K., 1126-1 Ichino-cho, Hamamatsu-shi 435-8558, Japan.

[19] Y. Unno *et al.*, "Development of n-on-p silicon sensors for very high radiation environments," *Nucl. Instrum. Meth. A,* in press, doi: 10.1016/j.nima.2010.04.080.

[20] T. Mäenpää *et al.*, "Silicon beam telescope for LHC upgrade tests," *Nucl. Instrum. Meth. A,* vol. 593, pp. 523-529, 2008.

[21] M. J. Kortelainen, T. Lampen, H. Moilanen and T. Mäenpää, "Off-line calibration and data analysis for the silicon beam telescope on the CERN H2 beam," *Nucl. Instrum. Meth. A,* vol. 602, pp. 600-606, 2009.

[22] M. J. French *et al.*, "Design and results from the APV25, a deep sub-micron CMOS front-end chip for the CMS tracker," *Nucl. Instrum. Meth. A,* vol. 466, pp. 359-365, 2001.

[23] V. Cindro *et al.*, "Radiation damage in p-type silicon irradiated with neutrons and protons," *Nucl. Instrum. Meth. A,* vol. 599, pp. 60-65, 2009.

[24] A. Zoboli *et al.*, "Functional characterization of p-on-n 3D-DDTC detectors fabricated at FBK-IRST", *IEEE Nuclear Science Symposium and Medical Imaging Conference (NSS - MIC'08), Conference Record,* paper N34-4, Dresden (Germany), October 19-25, 2008.

[25] R. Van Overstraeten and H. De Man, "Measurement of the ionization rates in diffused silicon p-n junctions," *Solid-St. Electron.* vol. 13, pp. 583-608, 1970.

[26] I. Mandić, V. Cindro, A. Gorišek, G. Kramberger, M. Mikuž and M. Zavrtanik, "Observation of full charge collection efficiency in heavily irradiated n+p strip detectors irradiated up to $3 \times 10^{15}\,\mathrm{n_{eq}/cm^2}$," *Nucl. Instrum. Meth. A,* vol. 612, pp. 474-477, 2010.

[27] J. Lange, J. Becker, D. Eckstein, E. Fretwurst, R. Klanner and G. Lindström, "Charge collection studies of proton-irradiated n- and p-type epitaxial silicon detectors," *Nucl. Instrum. Meth. A,* vol. 624, pp. 405-409, 2010.

[28] D. Pennicard *et al.*, "Synchrotron Tests of a 3D Medipix2 X-Ray Detector," *IEEE Trans. Nucl. Sci.,* vol. 57, no. 1, pp. 387-394, 2010.